Numerical simulation of bloodflow through elastic vessels

A de Bruin

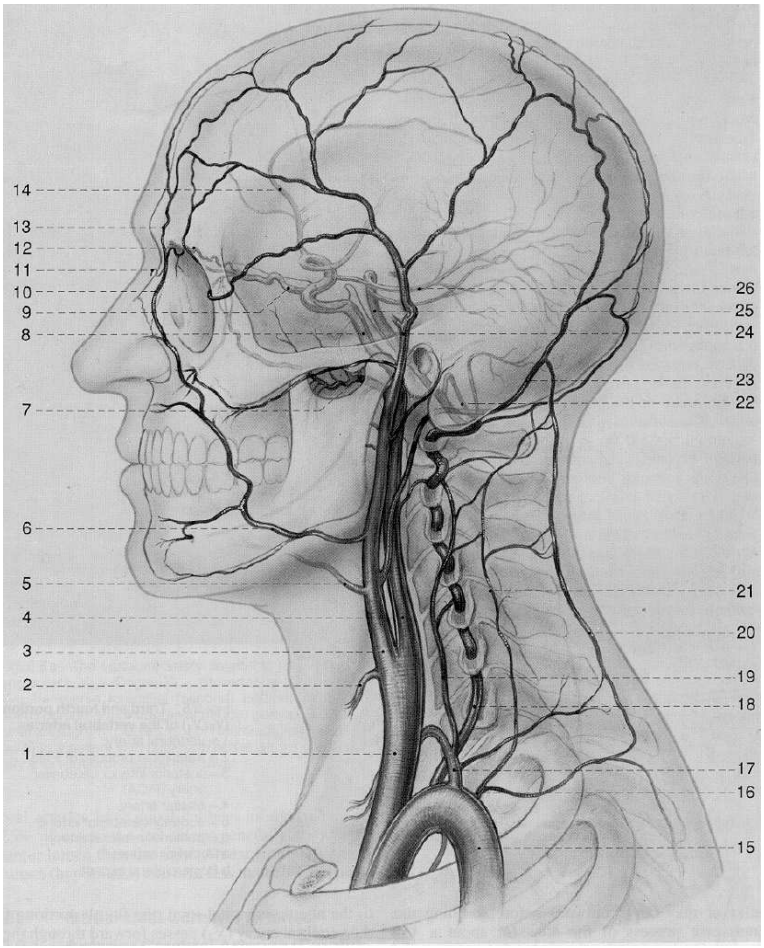

Department of Mathematics

RuG

Master's Thesis

Numerical simulation of bloodflow through elastic vessels

A de Bruin

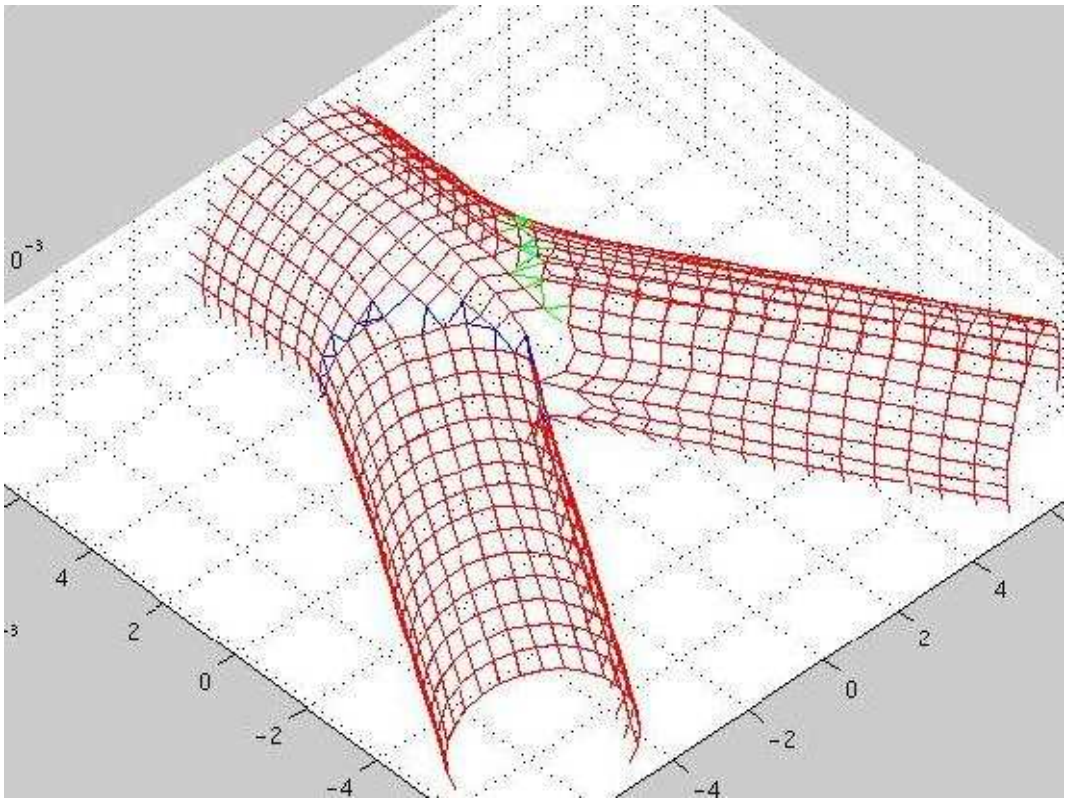

Supervisor:
Prof.dr. A.E.P. Veldman
Department of Mathematics
University of Groningen
P.O. Box 800
9700 AV Groningen

June 2003

Contents

Chapter 1

Introduction

The subject of the study is to simulate blood flow through arteries. This could be very usefull in the future in hospitals. For example, specialists could predict if a certain shape of an artery could cause a stenosis, and do something about it before people really get the stenosis.
This report handles about the simulation of blood flow through elastic arteries using a finite volume method. More precisely, the main subject of the study was to try to simulate blood flow with a geometry and velocity in realistic dimensions in both a straight elastic vessel as well as a bifurcated one.
During the last years the RuG has developed a finite volume code called ComFlo, see D.J. Kort [9] and E. Loots [13], which solves the complete Navier-Stokes equations in various different cases. For example, almost all geometries can be used and there is the possibility for in- and outflow as well as free surface flow. With this code blood flow can also be simulated by making the desired geometry and use the in- and outflow option. In this case the implementation of the elastic walls is tested for the first time.

In chapter 2 the mathematical model and the numerical model and the elasticity model that are used in Comflo are explained. In chapter 3 the results from simulations of straight and bifurcated vessels are discussed. Chapter 4 contains the conclusions of this report.

Chapter 2

Modeling

In this chapter we first explain the mathematical model of liquid flow with its boundary conditions that are necessary in the blood flow through tubes. After that, in section 2.2, the numerical model is explained. Section 2.3 is about the elasticity model which is used.

2.1 Mathematical model

Blood flow through arteries of course is a 3D flow. For any 3D flow domain filled with a Newtonian liquid (like blood in first approximation) the unsteady incompressible Navier-Stokes equations hold. These equations are given below.

- Firstly, we have the equation expressing the conservation of mass:

$$\frac{\partial u}{\partial x} + \frac{\partial v}{\partial y} + \frac{\partial w}{\partial z} = 0$$

  Here u, v and w denote the velocities in the $x-, y-$ and $z-$direction.

- Secondly, we have the equations expressing the conservation of momentum in x-, y- and z-direction, respectively:

$$\begin{aligned}
\frac{\partial u}{\partial t} + u\frac{\partial u}{\partial x} + v\frac{\partial u}{\partial y} + w\frac{\partial u}{\partial z} &= -\frac{\partial p}{\partial x} + \nu(\frac{\partial^2 u}{\partial x^2} + \frac{\partial^2 u}{\partial y^2} + \frac{\partial^2 u}{\partial z^2}) + F_x \\
\frac{\partial v}{\partial t} + u\frac{\partial v}{\partial x} + v\frac{\partial v}{\partial y} + w\frac{\partial v}{\partial z} &= -\frac{\partial p}{\partial y} + \nu(\frac{\partial^2 v}{\partial x^2} + \frac{\partial^2 v}{\partial y^2} + \frac{\partial^2 v}{\partial z^2}) + F_y \\
\frac{\partial w}{\partial t} + u\frac{\partial w}{\partial x} + v\frac{\partial w}{\partial y} + w\frac{\partial w}{\partial z} &= -\frac{\partial p}{\partial z} + \nu(\frac{\partial^2 w}{\partial x^2} + \frac{\partial^2 w}{\partial y^2} + \frac{\partial^2 w}{\partial z^2}) + F_z
\end{aligned}$$

  In these equations, t denotes the time, p the pressure scaled by the density, ν the kinematic viscosity and $\mathbf{F} = (F_x, F_y, F_z)^T$ the external body force. Since our simulation does not include an external body force, it will be omitted from now on.

With $\mathbf{u} = (u, v, w)^T$ these equations can also be denoted as:

$$\nabla \cdot \mathbf{u} = 0 \tag{2.1}$$

$$\frac{\partial \mathbf{u}}{\partial t} + (\mathbf{u} \cdot \nabla)\mathbf{u} = -\nabla p + \nu(\nabla \cdot \nabla)\mathbf{u} \tag{2.2}$$

Of course these equations need boundary conditions. The blood cannot flow through the wall and due to its viscosity it sticks to the wall. This yields at the wall:

$$u = 0 \quad \text{and} \quad v = 0 \quad \text{and} \quad w = 0$$

The pulsatile flow of the blood is simulated at the inlet of the artery by pushing it in. The blood volume to be pushed in can be controlled by the area of the inflow cross section and the blood velocity at the inlet. Therefore we have the inflow condition:

$$\mathbf{u}(x, y, z, t) = \mathbf{u}_{in}(t) \text{ at inlet}$$

At the outlet we prescribe the fluid to be unidirectional and the pressure to be equal to the pressure outside of the fluid :

$$\frac{\partial \mathbf{u}}{\partial \mathbf{n}} = 0 \quad \text{and} \quad p = p_0$$

Here $\mathbf{n} = (n_x, n_y, n_z)$ is the outward pointing normal at the outflow boundary.

Other conditions at the inlet and outlet are also possible. The inflow could be described as a fully developed flow and at the outlet the condition $-p\mathbf{n} + \frac{1}{Re}\frac{\partial \mathbf{u}}{\partial n} = 0$ could be imposed. However, the conditions imposed have been proved very useful in other simulations and are already implemented in ComFlo.
The used conditions need an extra long tube. The development of the flow needs time and length. Therefore, at the inlet of the simulated artery, a fully developed Poisieulle-flow is prescribed. The outflow also has a small effect on the flow near the end of the tube needing an extra bit of tube at the end of the simulated artery. So don't bother the results at the ends of the tube.

2.2 Numerical model

For the computations of the blood flow the computational grid is decomposed into five different kinds of cells: boundary cells, interior cells, exterior cells, inflow cells and outflow cells. In figure 2.1 a part of our cartesian grid and the geometry of section 3.2 are displayed. The different cell types can be found here also.
The exterior cells play no role in the discretization process, so they will not be mentioned here again.
The grid used is totally staggered. All the velocities are placed in the middle of the lateral faces of the cells and the pressures are placed in the centres of the cells. Now

the Navier-Stokes equations have to be discretized. The projection method is used here. This is an explicit method using the abrevation:

$$\mathbf{R}^n = -\nabla(\mathbf{u}^n \mathbf{u}^{nT}) + \nu \nabla \cdot \nabla \mathbf{u}^n$$

Now we split equation (2.2), the conservation of momentum, into two pieces using u^* and discretize them in time using forward Euler:

$$\begin{aligned} \frac{\mathbf{u}^* - \mathbf{u}^n}{\delta t} &= \mathbf{R}^n \\ \frac{\mathbf{u}^{n+1} - \mathbf{u}^*}{\delta t} &= -\nabla p^{n+1} \end{aligned}$$

Here δt is the time step and n and $n+1$ denote the old and the new time level.

When we add these two equations, the u^* vanishes and the result are the time discretized Navier-Stokes equations:

$$\frac{\mathbf{u}^{n+1} - \mathbf{u}^n}{\delta t} = \mathbf{R}^n - \nabla p^{n+1} \tag{2.3}$$

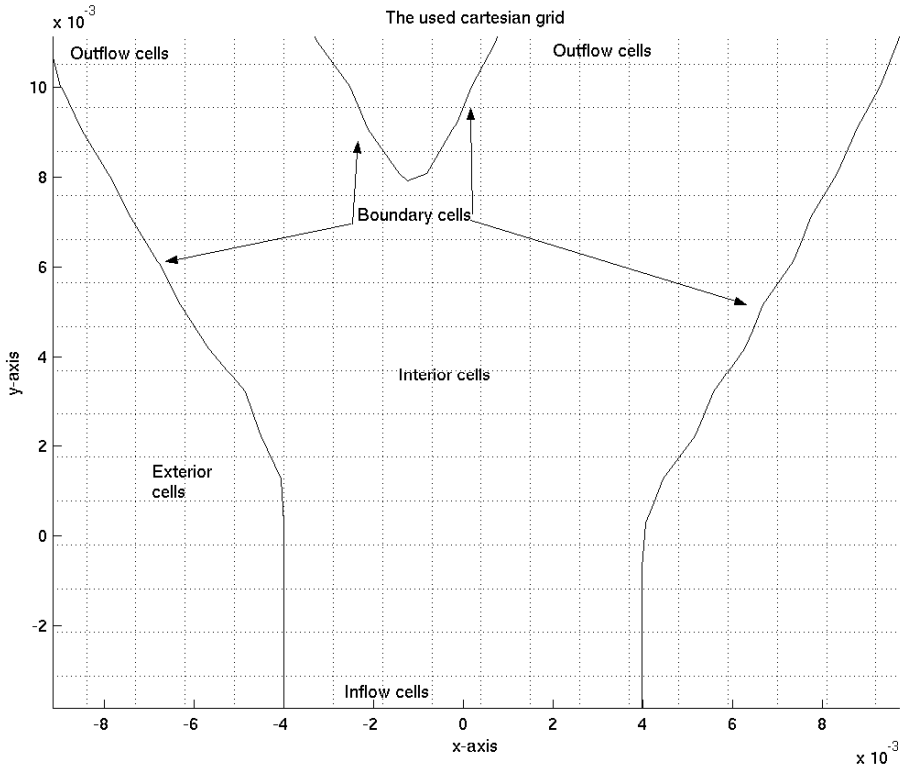

Figure 2.1: The used cartesian grid with the different cell types.

$$\nabla \cdot \mathbf{u}^{n+1} = 0 \tag{2.4}$$

We have to discretize in space too. This discretization can only be made for interior cells. First the discrete versions of the divergence and the gradient operators have to be defined. The divergence operator $\nabla\cdot$ becomes D_h and the gradient operator ∇ becomes G_h. In both cases h denotes the spatial step. Because we only discretize in interior cells, this has to be expressed in the divergence operator as well: $D_h = D_h^F + D_h^B$. The F represents here the inner flow domain and the B the boundary. Because of the unknown boundary velocities the complete discretization becomes

$$\begin{aligned} D_h^F \mathbf{u}^{n+1} + D_h^B \mathbf{u}^{n+1} &= 0 \\ \mathbf{u}^{n+1} &= \mathbf{u}^n + \delta t \mathbf{R}_h^n - \delta t G_h p^{n+1} \end{aligned}$$

By substitution of the second into the first equation, the pressure Poisson equation is obtained:

$$D_h^F G_h p^{n+1} = D_h^F (\frac{\mathbf{u}^n}{\delta t} + \mathbf{R}_h^n) + D_h^B \frac{\mathbf{u}^{n+1}}{\delta t} \tag{2.5}$$

This equation is solved, with the SOR method, and we can obtain the velocity field by substituting the pressure into equation (2.3).

Finally we have to look at the boundary, where the velocities are set to satisfy $\mathbf{u}= 0$ at the wall. This is done by interpolation and the use of mirror points.
This method is stable in the onedimensional case if:

$$\text{CFL} = \frac{U_{max}\delta t}{h} < 1 \quad \text{and} \quad \nu \frac{\delta t}{\delta x^2} < \frac{1}{2}$$

2.3 Elasticity model

Since the we have to regard the main application of our structure, i.e. blood vessels in general, we first consider the a priori assumptions we may or may not make.

- **Shape** Regarding the total vascular system, the largest part consists of cylinder-like structures. That means that we can, at first, describe a typical vessel as a cylinder, i.e. it is axisymmetric. The radius, however, can change, both in place (in axial direction), and, less apparent, in time. Unfortunately, such an approach, which is in fact 2D, does not allow to model topological changes like bifurcations (although, with some effort, curved vessels can in principle be modeled this way). Therefore, the model should be fully three-dimensional to capture these important features.

- **Thickness** We assume that the wall thickness is small and constant. In this case we may treat the wall as a *shell*. It is sufficient to indicate the position of the inner side of the vessel.

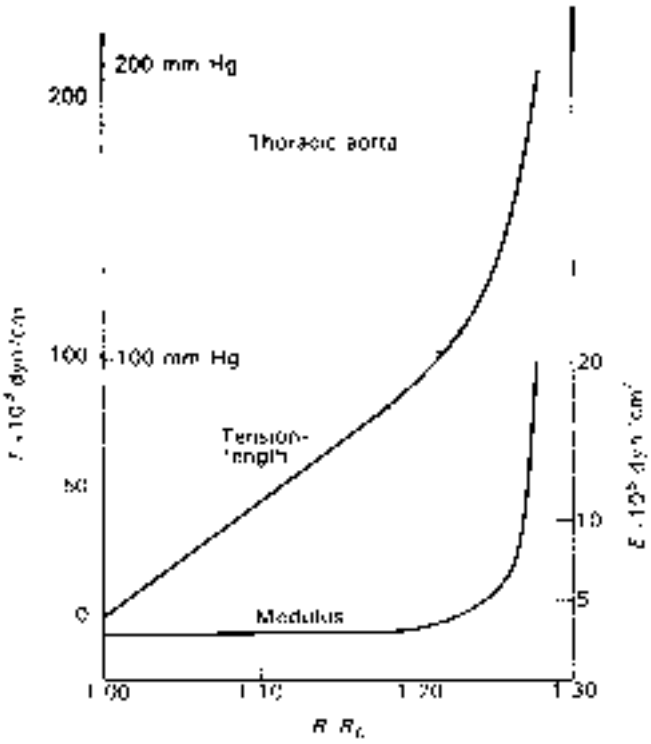

Fig. 10.5. The tension–length relation (elastic diagram) of a segment of the thoracic aorta of a dog subjected to various distending pressures Ordinate—tension in dynes × 10^3/cm (from eqn. 10.20), Abscissa—relative increase of radius (and hence of circumference).

The curve for the Young's modulus is plotted from the slope of the elastic diagram (tangent modulus). If the modulus were calculated with reference to the resting length at zero tension the value at 200 mm Hg pressure would be about 4·2 × 10^6 dynes/cm^2. This discrepancy between the two methods only becomes noticeable when there is a marked departure from linearity—for pressures up to 100 mm Hg the elastic behaviour, in this case, is remarkably linear.

Figure 2.2: *Tension-length relation of a segment of the thoracic aorta of a dog subjected to various distending pressures. The Young's modulus is also shown (lower line). After MacDonald [16].*

- **Material properties** The vessel is considered to consist of a homogeneous material. So we neglect the multiple-layer structure described above. That enables us, in principle, to forget about the thickness and replace the shell by a *membrane*, although without ignoring the stiffness properties of the shell.

We will therefore first take a look at the observed elastic behaviour of real vessel walls. Our main source are the experiments described by MacDonald [16]. For obvious technical reasons, measuring stress-strain relationships in an excised artery is much easier than measuring them in a living subject. Post-mortem changes, however, are limited because the collagen and elastin fibres are chemically very stable.

Firstly, in *longitudinal* direction, blood vessels are stretched; the rest length of a vessel is about 60% of its *in vivo* length, at least for young subjects. With increasing age, the retraction of a vessel, when dissected, reduces considerably.

Secondly, we take a look at the circumferential elasticity. In figure 2.2 the graph of distending pressure against the radius for a piece of artery is shown. It should be noted that this graph represents an *equilibrium*: it gives information in which way the transmural pressure force $\mathbf{F}_p$ balances the elastic, contracting circumferential force, $\mathbf{F}_s$ of the wall.

The Young's modulus, defined as the ratio of stress to strain, can simply be derived from this figure: it is the slope of the graph. Since the slope is not constant, it is common to speak of the *incremental* Young's modulus, which means the Young's modulus for a certain region in the graph where the stress/strain relation is locally considered linear. Note that there is a difference between the *pressure* and the *tension* because of the curvature; their relation is that pressure equals tension times radius, see below.

We will work out the radial elastic behaviour of the vessel wall; it will be shown that, and why, Hooke's law of linear elasticity does not hold here.

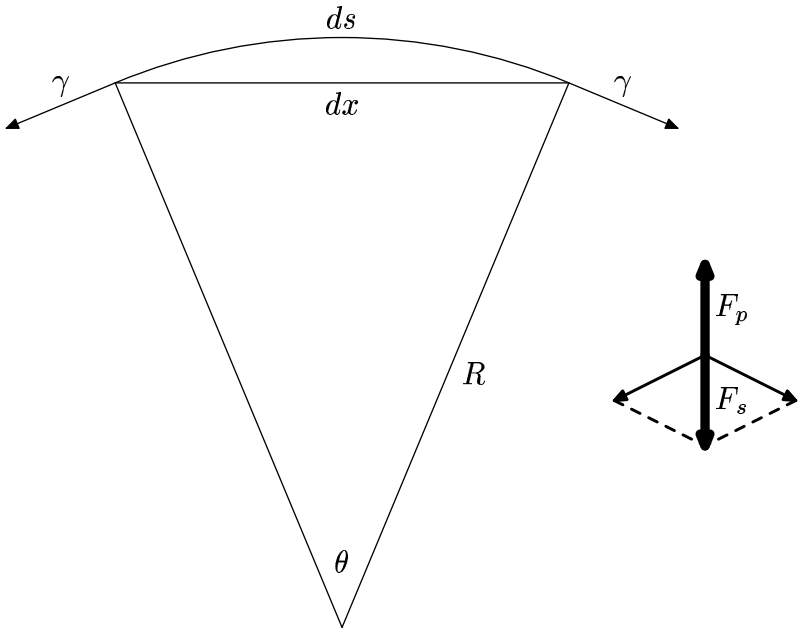

Figure 2.3: *Balancing of forces on a circular segment of a tube.*

Consider a small circular segment shown in figure 2.3 . The local pressure force is

$$\mathbf{F}_p^l = \Delta p \cdot A \quad = \quad \Delta p \cdot dx = \Delta p \cdot 2R \sin \frac{1}{2}\theta \approx \Delta p\, \theta\, R.$$

The pressure force has the same direction as the outward pointing normal.

Regarding the elastic properties, a force γ is exerted on both sides of the surface element because the surfaces next to the element try to shorten themselves. The resulting elastic force is

$$\mathbf{F}_s^l = 2\gamma \sin\frac{1}{2}\theta = \gamma\,\frac{dx}{R} \approx \gamma\,\theta.$$

This force is directed inwards.

Now suppose first that the structure behaves like a purely elastic material: $F = \alpha \cdot u$. For convenience, we consider the relative displacement $u = \frac{x-x_0}{x_0}$ instead of $u = x - x_0$ where x_0 is the rest length. On our surface element this leads to

$$\gamma = \alpha\left(\frac{ds - ds_0}{ds_0}\right) = \alpha\left(\frac{R\theta - R_0\theta}{R_0\theta}\right) = \alpha\left(\frac{R - R_0}{R_0}\right) \quad \text{and}$$

$$\mathbf{F}_s^l = \alpha\,\theta\,\frac{R - R_0}{R_0}. \tag{2.6}$$

Balancing the forces leads to the equilibrium

$$\mathbf{F}_p^l = \mathbf{F}_s^l \Longrightarrow \Delta p = \frac{\alpha}{R}\left(\frac{R - R_0}{R_0}\right) = \frac{\alpha}{R_0}\left(1 - \frac{R_0}{R}\right). \tag{2.7}$$

It means that equilibria with arbitrarily high values of R can be reached by letting Δp tend to $\frac{\alpha}{R_0}$. (This is immediately clear by observing in figure 2.4 that $\mathbf{F}_p^l$ and $\mathbf{F}_s^L$ are linear functions of R; their intersection point goes to infinity as their slopes approach each other.)

This is a highly unstable situation where 'blow outs' can easily occur when the pressure is increased; nevertheless, it represents exactly the behaviour of, say, a balloon. (This phenomenon is also linked to the well-known 'Law of Laplace', in its simplest form given as $\Delta p = \frac{c}{R}$, which states that the required pressure to distend a tube against a given tension in the wall is reciprocal to the radius of the tube.)

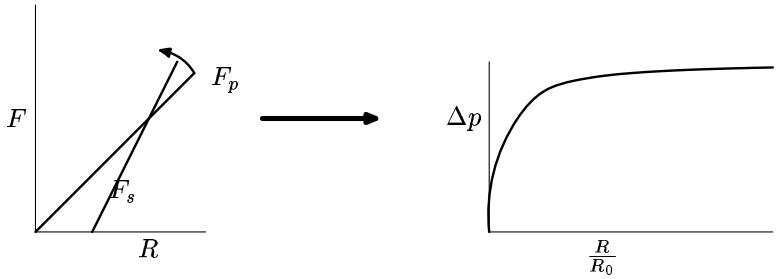

Figure 2.4: *Pressure/strain curve in the linear elastic case. A modest increase of the pressure force (left-hand figure), causes a large growth of the radius (right-hand figure).*

Returning to figure 2.2 we see a *vertical* asymptotic behaviour instead, representing the fact that at higher strains the surrounding material (collagen fibres) supports the stress; a commonly made analogy is that of the balloon being in a string bag.

From the experimental results as shown in this figure we obtained the following relationship:

$$\Delta p\, R = 133[(1-\omega)f_1 + \omega f_2];$$
$$f_1 = 444(\frac{R}{R_0} - 1); \quad f_2 = 22.4(1.3 - \frac{R}{R_0})^{-0.6}$$

(the factor 133 represents the conversion from the standard use of $mm\,Hg$ in medical sciences to SI units) and where ω is an indicator function:

$$\omega = I_{\frac{R}{R_0}>1.18}$$

Let us return to figure 2.2. The *in vivo* range of arteries in terms of $\frac{R}{R_0}$ lies between 1.17 and 1.24, exactly where the graph starts to bend upwards. This has to be taken into account in numerical simulations; both initially stretched walls in circumferential direction and an adequate pressure difference have to be provided. Alternatively, it is possible to linearize around an equilibrium and use the locally constant incremental Young's modulus.

The elastic properties described above hold only for a specific artery but are similar in most medium- and large-sized vessels. Other elastic structures in the body behave differently. As an example consider the left ventricle of the heart, which can roughly be described as an ellipsoidal-like object. The stress-strain relationship in radial direction (and neglecting the axial direction) is, according to Janz and Grimm [8]:

$$\gamma = \frac{4Eh}{3\alpha}\sinh\alpha\epsilon, \tag{2.8}$$

where ϵ is the strain, or the $\frac{ds-ds_0}{ds_0}$ in figure 2.3 ; E is the incremental Young's modulus and h the thickness of the ventricle wall. α is here an nonlinearity parameter; note that for small values of α and ϵ, equation (2.8) boils down to

$$\gamma = \frac{4}{3}\,E\,h\;\epsilon = \beta\frac{s-s_0}{s_0},$$

i.e. the same linear relationship we have seen earlier in equation 2.6.

Chapter 3

Simulations

In this chapter various simulations using ComFlo are discussed.
In section 3.1 we simulate flow through a straight elastic vessel. We used Pedrizetti's [18] results to tune our parameters of elasticity α and β because the exact physical meaning of our parameters is not yet known.
Pedrizetti simulated the flow through a straight vessel in which only the middle 1/3 section has an elastic wall. He used a vessel diameter of 0.5 cm and a velocity of about 0.5 $\frac{m}{s}$. He used an elasticity parameter equal to the average of human arteries. The Reynolds number is kept fixed at 300. In our simulations we used the same vessel size and inflow speeds as Pedrizetti to make sure that we are doing the same simulation.
Only Perdrizetti didn't use an elasticity model like us, but he used the membrane equations. A membrane is a mathematical model for the solid shell of extremely small thickness such that it can be assumed as having no bending stiffness. A membrane suppports only stresses parallel to its surface which are also assumed to be constant along the thickness. In the present work the membrane is assumed inertialess. Such an assumption means that the total membrane mass is negligible with respect to the mass of the fluid which accelerates during the motion. It has been verified in the limit of extremely small membrane thickness (see Luo [14]). In such a scheme the membrane deforms to be constantly in equilibrium with the external loads.
In section 3.2 simulations in a bifurcated vessel have been done. The different grid sizes, the marker distances and the wall shear stress will be discussed.

3.1 Straight vessel

In this section we use the steady state of Pedrizetti to tune our elasticity parameters α and β, see Loots [15]. The relation between α and β and the Young's modulus can also be found in [15]. Many simulations have been done using various different parameters. Finally we've got the same results for the geometry as Pedrizetti. This happened for $\alpha = 5 \cdot 10^{-2}$ and $\beta = 50$, so we use these values in further simulations.

Important in all simulations is that α is not choosen too high and β too low. $\alpha = 0$ corresponds with no elasticity and $\beta = 0$ with no damping. When elasticity is used, it is important that when the wall expands the parameter $\beta > 0$ pushes the wall back towards its original shape. Otherwise the vessel will keep expanding until the geometry is the same size as the overall computational domain which will make the program crash.
In figure 3.1 the geometry of Pedrizetti after extending is plotted along with some streamlines. In figure 3.2 the geometry of ComFlo is plotted. The surface here is not very smooth because a coarse grid is used. Although the tube of Pedrizetti is 2.5 times narrower, in both pictures it can be seen that the extension of the tube is about 20%. The length of the bump is in Pedrrizetti's case also 2.5 times smaller than in the ComFlo case.

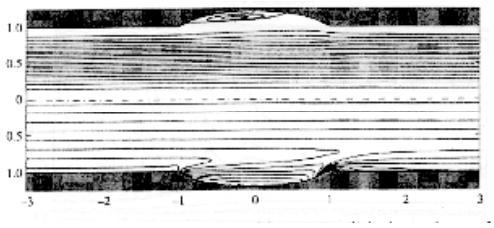

Figure 3.1: The geometry of Pedrizetti.

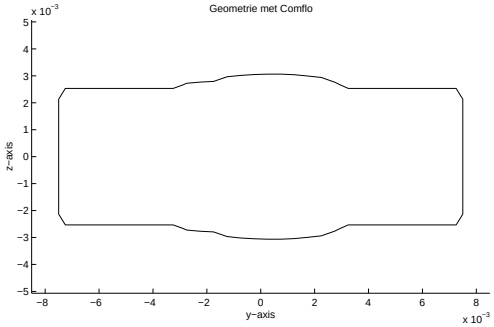

Figure 3.2: The geometry with ComFlo.

Now we want to compare the results between three grids. The first has a coarse grid of 15X15X30 points. The others have respectively a 22X22X45 and a 30X30X60 grid.
In figure 3.3 the volume of the vessel is plotted as function of the time. Because the inflow is constant in time there will be a balance accomplished in which the volume is constant.
Then there is the point of the difference between the equilibrium volumes at $t = 1.0s$. This equilibrium is an approximation of the real volume. For the same reason, the volume of the vessel in the fine grid is most likely the most exact value because the steps in volume are much smaller due to the fine grid.
The next topic to investigate is the influence of the number of elasticity markers. I used numbers of elasticity markers from 1800 to 6000 on the same grid. The results were almost equal to each other, as can be seen in figure 3.4.
Just be sure you always use a marker distance comparable with the size of the cells, but not too small so that the calculations will not take more time than neccessary. If you choose it too large the program will not run, see Loots [15].
Usually the same number of markers as there are cells are taken in the axial directions. In circumferential direction three times the number of cells in x- and z-

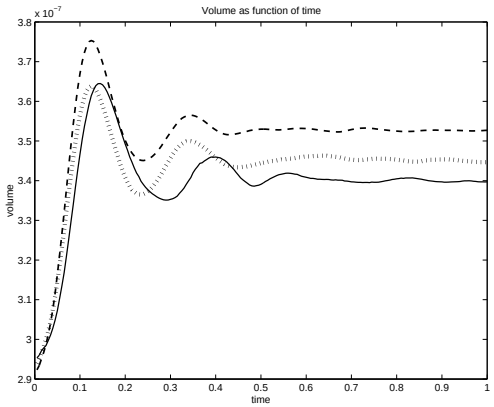

Figure 3.3: The volume as function of the time for a constant inflow. Dashed line for the coarse grid, the dotted line for the medium grid and the solid line is for the fine grid.

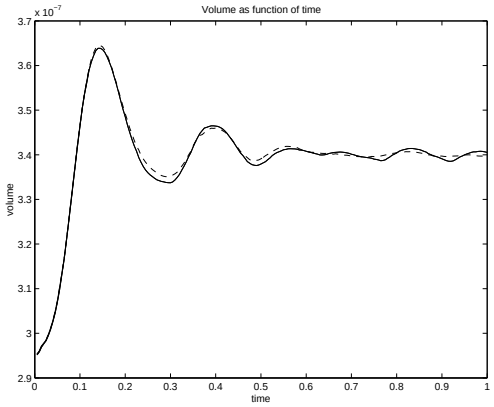

Figure 3.4: The volume as function of the time for a constant inflow. Dashed line for the small numbers of markers.

direction can be taken. The maximum radius of the vessel is equal to half the number of cells in the x- or z- direction, which makes a circumference of $\pi * \#$ cells.

3.2 Bifurcated vessel

With the elasticity parameters derived from the first simulations we want to simulate the flow through a bifurcated vessel. The geometry is made from three tubes connected by a handmade surface as can be seen in figure 3.5.
The following three topics will be discussed in the three subsections:

- The influence of the number of markers.
  Regarding the previous section we don't expect much difference provided we don't use too few markers.
- The influence of the number of cells.
  Most likely, a finer grid will give better details, but a longer computation time. Too few cells will give a too rough approximation.
- The wall shear stress.
  This topic is interesting for the medical world because a low wall shear stress can cause plaque in an artery.

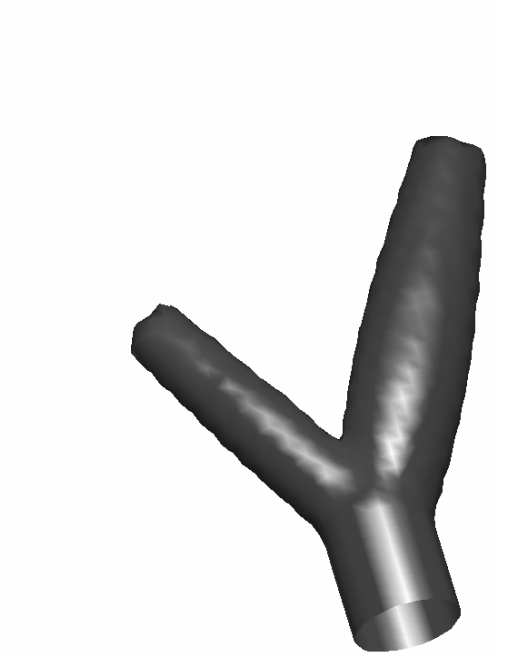

Figure 3.5: Three dimensional geometry of the bifurcated vessel.

3.2.1 Elasticity markers

First we look at the number of markers, which were explained in section 2.3. Simulations have been done for a 90X90, a 70X70 and a 55X55 grid of springs. These

are the number of springs in axial and circumferential direction of each tube. A pulse similar to a heartbeat is used for the inflow. The flux, i.e. the volume liquid that passes the inlet, is plotted in figure 3.6. The interesting moments in time that will be highlighted in the simulation results are drawn in this picture. From here on, they will be named Acceleration Phase (AP), Deceleration Phase (DP) and End Diastolic phase (ED).

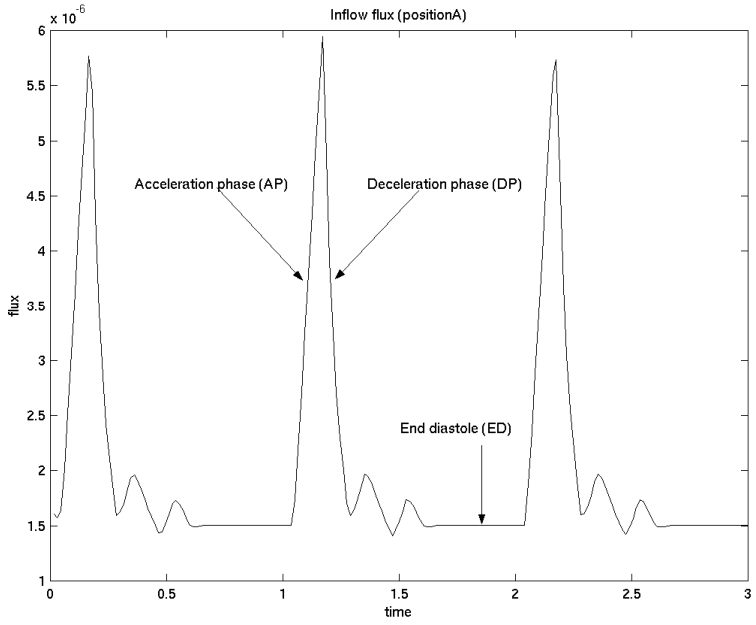

Figure 3.6: Inflow flux for the simulations with the bifurcated vessels

The figures 3.7 up to 3.9 show the geometry after 1 second of simulation for the various numbers of markers. For a good simulation the springs must be 'shorter' than a grid cell. So in the axial direction there should be at least the same number of springs as cells in the y-direction.
For the radial direction it is a bit more complicated. The number of springs should be more then $\pi *$number of cells in the other directions. In figure 3.9 it is clearly visible what happens when you use too few markers: The wall of the artery has not-expected bumps and is no longer smooth.
Although they have different numbers of markers, figures 3.7 and 3.8 show the same geometry. Therefore it is expected that the number of markers does not influence the simulation (if you use enough markers).
This is also visible in figure 3.10 where the volume of the vessel is plotted as function of the time. The large peaks are of course the moments when the heart beats and pushes fluid into the vessel so that it expands.

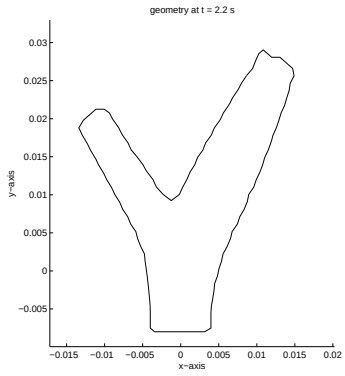

Figure 3.7: Geometry in case of small marker distance.

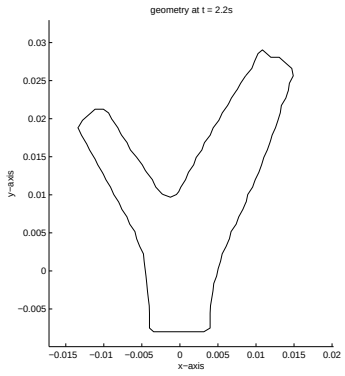

Figure 3.8: Geometry in case of medium marker distance.

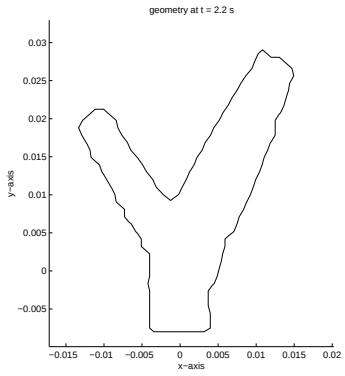

Figure 3.9: Geometry in case of large marker distance.

The only noticeable difference between the three simulations is that the simulation with the least number of markers lies a little bit higher than the other two. This is most likely a result of the bumps seen in figure 3.9.

3.2.2 Grid refinement

In this section the influence of different grid sizes is discussed. The three different grids used are a 60X40X20, a 46X30X16 and a 30X20X12 grid. Again we will look at the volume as a function of time for the various grid sizes. Next the differences

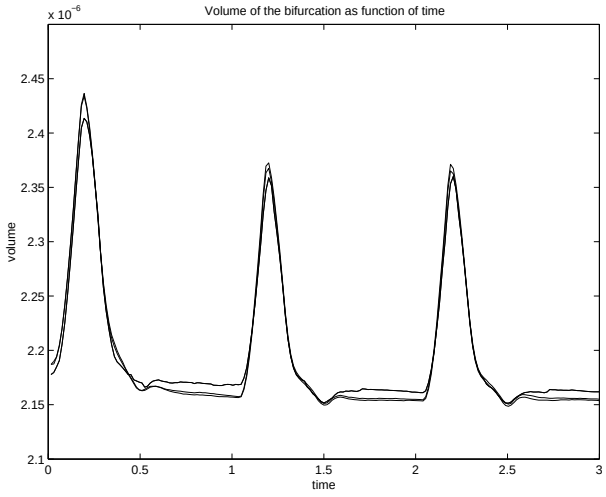

Figure 3.10: The volume as function of time for a pulsatile inflow for various numbers of markers.

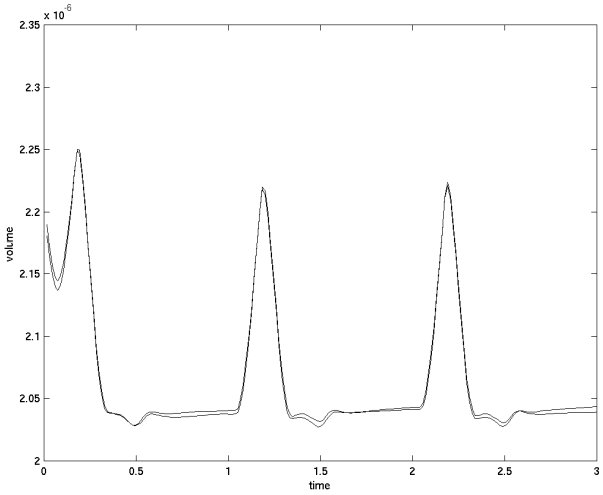

Figure 3.11: The volume as function of time for a pulsatile inflow for three different grid sizes.

of the shape af the geometry in the different grids and at different moments in time will be discussed.
In figure 3.11 the different volumes for the three simulations are plotted as a function of time. There is almost no difference between the various grids. So the amount of liquid flowing through the bifurcation is equal for the three grids.
Figure 3.13 shows the velocity profiles of respectively the acceleration, the deceleration and the end diastolic phase. Each of the figures contains three plots of respectively the inlet, the right outlet and the left outlet. These three places can be seen in figure 3.12 as position A, B and C.
Instead of figure 3.11, figure 3.13 gives us visible difference between the coarse grid and the other two, especcially at the two outlets. Therefore a 30X20X12 grid is too coarse for this case.

3.2.3 Wall shear stress

Wall shear stress is a very important subject when we are talking about stenoses. Area's of the vessel wall with low wall shear stress are vulnerable for stenoses. Wall shear stress is defined as the length of the vector $(\frac{\partial u}{\partial \mathbf{n}} \frac{\partial v}{\partial \mathbf{n}} \frac{\partial w}{\partial \mathbf{n}})$. In figure 3.14 the wall shear stress is plotted. In these pictures it is visible that especcially the left and right wall just before the bifurcation have low wall shear stress and thus are vulnerable for stenosis.

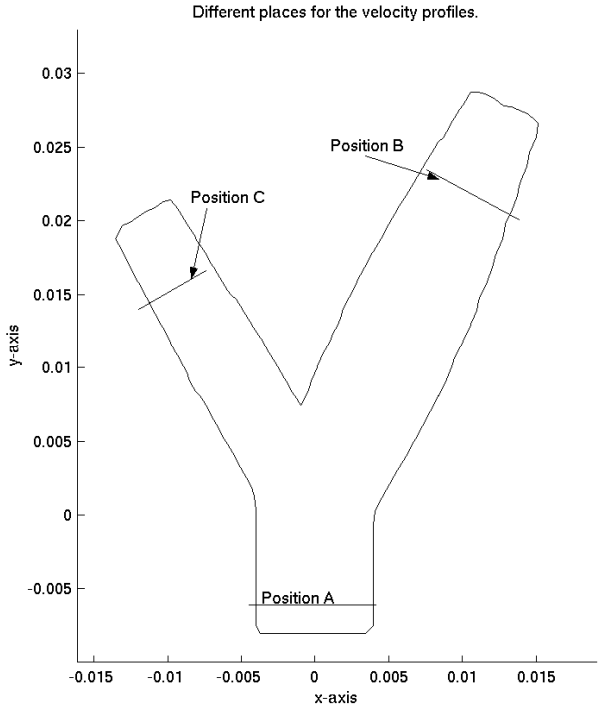

Figure 3.12: The positions A, B and C where the velocity profiles have been plotted.

3.2.4 Conclusions

Again there is not much difference for the volume between the various grids. The velocity profiles are almost equal at the inlet as expected because that is where the velocity is prescribed. However, the simulation with the coarse grid gives quite different results for velocity profiles at the two outlets. Looking at the differences between the results we may conclude that using the 30X20X12 grid has too large cells to make a good simulation of this flow problem. However, the results from the other two grids (46X30X16 and 60X40X20) are almost equal so that we may say that the grid does not have to be more refined in this case. This is interesting because for future practical use, the computing time must be very small. For example when you double the number of cells in all directions, the computing time will be eight times as large if you are using the same time step. Unfortunately, smaller cells will increase the CFL-number which must be smaller than 1 for convergence. So when the number of cells is doubled in each direction, the time step has to be two times as small, hence the simulation will take 16 times as much time.

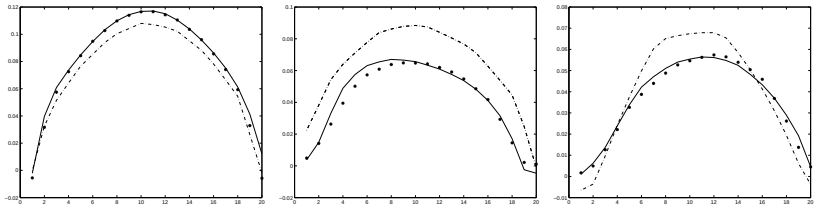

Velocity profiles in the Acceleration Phase

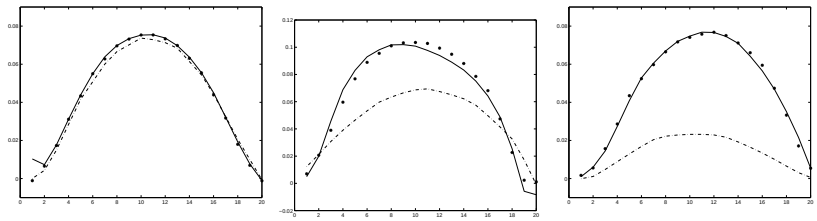

Velocity profiles in the Deceleration Phase

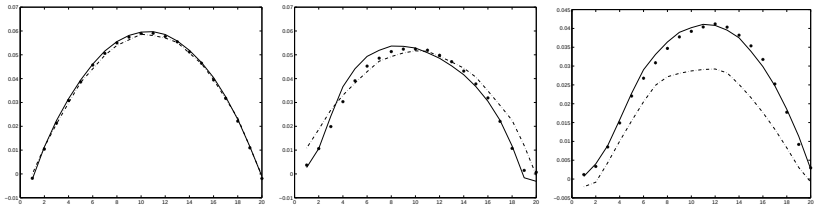

Velocity profiles in the End Diastole.

Figure 3.13: Solid line for the fine grid, stars for the medium grid and line-point for the coarse grid. Columns from left to right resp. positions A, B and C.

The wall shear stress gives pictures which were expected. In the beginning of the bifurcation is the largest chance to get a stenosis. This was also discovered in measurements of living patients, see Taylor [23].

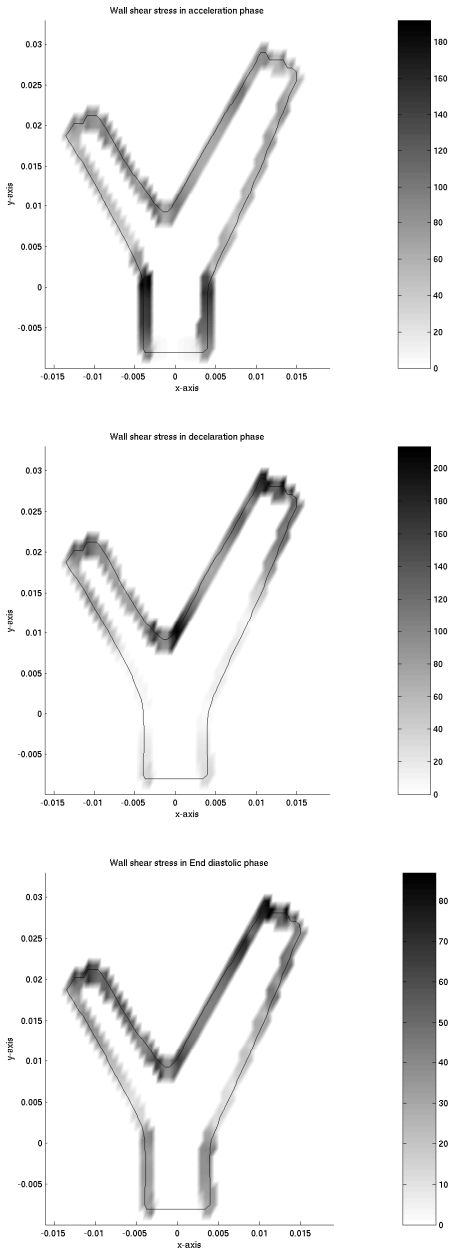

Figure 3.14: Wall shear stress for resp. AP, DP and ED

Chapter 4

Discussion

As for so many other flow problems, $ComFlo^{©}$ can be used to solve problems of flow through elastic tubes. In this report simulations have been performed for a straight elastic vessel and a bifurcated one.
The results from the first simulation yield values for the elasticity parameter corresponding to the elasticity of a human artery.
With these values simulations have been made for a bifurcated vessel. Three topics were discussed:

- marker distance refinement
- grid refinement
- the wall shear stress

There is a minimum number of markers for the program to run, but further refinement won't give better results. This minimum is in axial direction equal to the number of cells and longitudinal direction and in radial direction equal to the $\pi \cdot$#cells in the vessel in one of the two other direction.
As for many numerical problems grid refinement influences the results. We've seen unexpected velocity profiles for the coarse grid. So always use enough cells in your geometry, in this case 46X30X16 should be enough.
In the last subsection the wall shear stress is discussed. This is an important subject when talking about stenoses. From the figures we have seen that the areas on the wall left and right from the bifurcation have the lowest wall shear stress in all phases of the heart pulse, so there the chance of a stenosis is much larger then at other places of the artery wall.

For further development of the program the physical properties of arteries and blood could be better modelled. For example elasticity of an artery varies at the surface of the bifurcation, and the inner wall of an artery is not smooth but has a lot of small bumps that could influence the flow. Also blood is not just a fluid of a constant density but consists of cells which are much larger than molecules of course. Further

the inflow pulse will vary in different parts of the body and will always be more complicated than the function that is used here.

Bibliography

[1] M. Abramowitz, I. A. Stegun (1970): "Handbook of Mathematical Functions" Dover publications, Inc., New York.

[2] S. A. Berger, L-D. Jou (2000): "Flows in Stenotic Vessels" Annu. Rev. Fluid Mech. 2000. 32:347:382

[3] D. Bluestein, L. Niu, R. T. Schoephoerster, M. K. Dewanjee (1996): "Steady Flow in an Aneurysm Model: Correlation Between Fluid Dynamics and Blood Platelet Deposition" Journal of Biochemical Engineering, august 1996 p 280-286

[4] "BIACORE 2000 Instrument Handbook": Chapter 2 and Appendix A

[5] R. Budwig, D. Elger, H. Hooper, J. Slippy (1993): "Steady Flow in Abdominal Aortic Aneurysm Models". Journal of Biochemical Engineering, november 1993 p 418-423.

[6] R. Comolet (1982): "Mécanique Expérimentale des Fluides." Masson, Paris.

[7] Koen Goorman (2000): "Steady and unsteady channel flows, numerical models with applications to the recorder flute and vocal folds modeling". Master's Thesis TU Eindhoven

[8] R.F. Janz & A.F. Grimm (1973): "Deformation of the diastolic left ventricle - nonlinear elastic effects." Biophys. J., nr. 7 p. 509-516.

[9] Dirk-Jan Kort (2000): "Numerical Simulations of the blood flow in the arteria carotis communis: a pilot study". Unpublished report RuG

[10] P.-Y. Lagrée (2000): "An inverse technique to deduce the elasticity of a large artery." Unpublished report LMM Paris

[11] P.-Y. Lagrée & S. Lorthois (1999): "Interacting Boundary layer flow in a stenosis". Archives of Physiology and Biochemistry Vol 107 sept 99, p 51.

[12] P.-Y. Lagrée & M. Rossi (1997): "Modélisation de l'écoulement sanguin par une approche de type couche limite instationaire. Mise en oevre d'une méthode inverse pour trouver l'elasticité de la paroi et la viscosité du fluide." Unpublished report LMM Paris.

[13] Erwin Loots (1998): "Free Surface Flow in 3D Complex Geometries using Enhanced Boundary Treatment". Master's Thesis RuG

[14] X. Y. Luo, T. J. Pedley (1996): "A numerical simulation of unsteady flow in a two-dimensional collapsible channel." Journal for fluid mechanics Vol. 314. p. 191-225.

[15] Erwin Loots (2003): "Fluid-Structure Interaction in Hemodynamics". RuG.

[16] D. A. MacDonald (1960): "Blood flow in arteries." Arnold, London.

[17] Pedley T.J. (1980): "The fluid mechanics of large blood vessels", Cambridge University Press.

[18] Pedrizetti G. (1998): "Fluid flow in a tube with an elastic membrane insertion" Journal of Fluid Mechanics, Vol. 375, p. 39-64.

[19] Perktold K, Rappitsch R. (1994): "Computer simulation of local blood flow and vessel mechanics in a compliant carotid artery bifurcation model" Journal of Biomechanics, Vol. 28, No. 7, p. 845-856.

[20] Reuderink P.J. (1991): "Analysis of the flow in a 3D distensible model of the carotid artery bifurcation" Master's Thesis Technical University of Eindhoven.

[21] H. Schlichting (1987): "Boundary layer theory" 7th ed Mc Graww Hill.

[22] Siegel, J.M Markou, C.P. Ku, D.N. and Hanson, S.R (1994): "A scaling law for wall shear stress through an arterial stenosis", ASME Journal of Biomechanical Engineering 116, p. 446- 451.

[23] Taylor, C.A. Hughes, T.J.R. Zarins Z.K. (1997):"Finite element modeling of blood flow in arteries" Comput. Methods Appl. Mech. Engrg. 158 p. 155-196

[24] Veldman, A.E.P. "Grenslaagstromingen" Lecture notes RuG

[25] Young, D.F. (1979):"Fluid Mechanics of Arterial Stenoses". ASME Journal of Biomechanical Engineering 101, p. 157- 173.